

# The Gradual Release of Alendronate for the Treatment of Critical Bone Defects in Osteoporotic and Control Rats

Věra Hedvičáková<sup>1</sup>, Radmila Žižková<sup>1,2</sup>, Matěj Buzgo<sup>1,3</sup>, Lucie Vištejnová<sup>4</sup>, Pavel Klein<sup>4,5</sup>, Maria Hovořáková<sup>6</sup>, Martin Bartoš<sup>7,8</sup>, Klára Steklíková<sup>6</sup>, Jitka Luňáčková<sup>7</sup>, Eva Šebová<sup>1</sup>, Iveta Paurová<sup>4</sup>, Miroslava Rysová<sup>9</sup>, Eva Filová<sup>1</sup>, Michala Rampichová<sup>1</sup>

<sup>1</sup>Department of Tissue Engineering, Institute of Experimental Medicine, the Czech Academy of Sciences, Prague, Czech Republic; <sup>2</sup>Department of Chemistry, Faculty of Science, Humanities and Education, Technical University of Liberec, Liberec, Czech Republic; <sup>3</sup>BIOFABICS Lda, Porto, Portugal; <sup>4</sup>Biomedical Center, Faculty of Medicine in Pilsen, Charles University, Pilsen, Czech Republic; <sup>5</sup>Department of Pathological Physiology, Faculty of Medicine in Pilsen, Charles University, Pilsen, Czech Republic; <sup>6</sup>Institute of Histology and Embryology, First Faculty of Medicine, Charles University, Prague, Czech Republic; <sup>7</sup>Institute of Dental Medicine, First Faculty of Medicine and General University Hospital, Prague, Czech Republic; <sup>8</sup>Institute of Anatomy, First Faculty of Medicine, Charles University, Prague, Czech Republic; <sup>9</sup>Department of Applied Biology, Institute for Nanomaterials, Advanced Technologies and Innovation, Technical University of Liberec, Liberec, Czech Republic

Correspondence: Michala Rampichová, Department of Tissue engineering, Institute of Experimental Medicine, the Czech Academy of Sciences, Videnska 1083, Prague, 14220, Czech Republic, Tel +420 241 062 692, Email michala.rampichova@iem.cas.cz

**Purpose:** Osteoporosis is a severe health problem with social and economic impacts on society. The standard treatment consists of the systemic administration of drugs such as bisphosphonates, with alendronate (ALN) being one of the most common. Nevertheless, complications of systemic administration occur with this drug. Therefore, it is necessary to develop new strategies, such as local administration.

**Methods:** In this study, emulsion/dispersion scaffolds based on W/O emulsion of PCL and PF68 with ALN, containing hydroxyapatite (HA) nanoparticles as the dispersion phase were prepared using electrospinning. Scaffolds with different release kinetics were tested in vitro on the co-cultures of osteoblasts and osteoclast-like cells, isolated from adult osteoporotic and control rats. Cell viability, proliferation, ALP, TRAP and CA II activity were examined. A scaffold with a gradual release of ALN was tested in vivo in the bone defects of osteoporotic and control rats.

**Results:** The release kinetics were dependent on the scaffold composition and the used system of the poloxamers. The ALN was released from the scaffolds for more than 22 days. The behavior of cells cultured in vitro on scaffolds with different release kinetics was comparable. The difference was evident between cell co-cultures isolated from osteoporotic and control animals. The PCL/HA scaffold show slow degradation in vivo and residual scaffold limited new bone formation inside the defects. Nevertheless, the released ALN supported bone formation in the areas surrounding the residual scaffold. Interestingly, a positive effect of systemic administration of ALN was not proved.

**Conclusion:** The prepared scaffolds enabled tunable control release of ALN. The effect of ALN was proved in vitro and in in vivo study supported peri-implant bone formation.

**Keywords:** alendronate, co-culture, fibrous scaffold, osteoporosis, drug delivery system

## Introduction

Osteoporosis is a severe metabolic disease of bone connected with an imbalance in bone remodeling resulting in bone loss, damage to skeletal microarchitecture, and impaired bone strength. The International Osteoporosis Foundation reports that osteoporosis causes more than 8.9 million fractures annually worldwide. The cost of osteoporosis including pharmacological intervention in the EU in 2021 was estimated at €56.9 billion.<sup>1</sup> The healing of bone fractures in osteoporotic patients is complicated by poor bone quality, which can complicate fracture fixation and stability.<sup>2</sup>

The treatment of osteoporosis has necessitated medical care for several decades. In the last century, osteoporosis was treated mainly with estrogen,<sup>3</sup> calcitonin,<sup>4</sup> or calcium and vitamin D supplementation.<sup>5</sup> Nowadays, a broader spectrum of drugs is offered, such as an antibody against the receptor activator of nuclear factor kappa B ligand (RANKL) or sclerostin,<sup>6,7</sup> parathyroid hormone analog,<sup>8</sup> selective estrogen receptor modulator<sup>9</sup> or bisphosphonates (BPs).<sup>10</sup>

In general, BPs are compounds resembling a pyrophosphate structure. Therefore, BPs bind calcium ions with high affinity that become part of the bone. Subsequently, BPs are internalized by osteoclasts and they inhibit enzymes within the mevalonate pathway, resulting in an altered prenylation of proteins, affecting the bone resorption executed by osteoclasts.<sup>11</sup>

Alendronate (ALN) is a type of BPs that has been investigated in clinical trials over the decades. Oral administration of ALN increased bone mineral density, and decreased the risk of clinical fractures. However, over the years associated problems, such as osteonecrosis of the jaw, appeared.<sup>12</sup> Therefore, new directions, such as local administration of ALN, are being investigated.<sup>13,14</sup>

In bone tissue engineering, drug delivery-based approaches are at the center of interest because local delivery increases the efficacy of the drug on the targeted bone. A wide variety of scaffolds such as calcium phosphate cements,<sup>15</sup> mesoporous bioactive glass,<sup>16</sup> graphene oxide-related hydrogels,<sup>17</sup> porous titanium implants,<sup>18</sup> autogenous bone graft<sup>19</sup> or electrospun polycaprolactone (PCL),<sup>20</sup> have been tested as drug delivery systems for ALN.

The aim of the study was to investigate the effect of the drug delivery system releasing ALN from the electrospun scaffold on the healing of bone defects in osteoporotic conditions. The hypothesis behind this work is that if ALN is used at a concentration not harmful to the osteoblasts, bone formation will occur and at the same time osteoclasts that are more active in the osteoporotic conditions will be inhibited. The release of ALN will occur only locally for a limited time necessary for appropriate bone healing, therefore, eliminating the disadvantages associated with the oral administration of ALN.

In this study, a nanofibrous PCL scaffold with incorporated hydroxyapatite (HA), prepared by the electrospinning technique, served as a drug delivery system for ALN. The prepared scaffold was firstly tested *in vitro* to verify its biocompatibility. Moreover, the co-cultures of primary osteoblasts and induced osteoclasts isolated from control or osteoporotic animals were used for complex examination of the scaffold properties. Subsequently, the comprehensive *in vivo* study was performed. The effect of the scaffold releasing the ALN on the healing capacity of the bone was examined on the control and osteoporotic rats with or without systemic ALN administration.

## Materials and Methods

### Scaffold Preparation

Electrospun nanofibers were prepared using needleless electrospinning. 24% (w/v) PCL (45kDa, Sigma Aldrich) was prepared in a solution of chloroform and ethanol (9:1 ratio). In the samples with HA (~ 200nm particles, Sigma Aldrich), a dry powder was dispersed in PCL up to the final 20 wt% concentration. In the case of the nanofibers containing Pluronic 31R1 (P31R1; Sigma Aldrich), the surfactant was mixed with PCL in a concentration of 0.1 wt% of P31R1 to dry PCL. In the samples with ALN (Sigma Aldrich), an ALN solution of 5% (w/w) Pluronic F68 (PF68, Sigma Aldrich) was added to a concentration of 2 mg of ALN for 1 g of PCL, and emulsified using constant stirring. In the case of the samples without ALN, a pure PF68 solution was added. The final solutions were electrospun using the Nanospider NS500 electrospinning unit, applying a wire electrode and 0.6 mm flow dosage element. The temperature and humidity were kept at room temperature, and the overall potential was kept below 70 kV.

### Scanning Electron Microscopic Analysis of Scaffolds

A scanning electron microscopy (SEM) was performed to characterize the nanofibrous scaffolds. The nanofibers were cut into pieces, placed on SEM holders using conductive tape, and sputtered with a 10nm layer of gold. The SEM analysis using SED detector at -10 kV potential was performed on Phenom ProX electron microscope (ThermoScientific).

### Detection of Hydroxyapatite in the Scaffolds

Scaffolds were stained by Alizarin Red S staining (ARS, 8678, Merck) to detect HA. Scaffolds were visualized under the light microscope Olympus IX51 with a digital camera DP80.

A Fourier transform infrared spectrometer (FTIR) (iZ10, Thermo Fisher Scientific) with ATR on diamond crystal was used to obtain infrared spectra of the nanofibers. The scans (8/8 background/sample scans) were recorded between  $4000\text{ cm}^{-1}$  and  $400\text{ cm}^{-1}$  with correction on atmospheric suppression, baseline correction and normalized scale. Obtained spectra were compared to spectral library on pristine components and PCL nanofibres.

The thermal properties of electrospun nanofibers were studied by thermogravimetric analysis (TGA) (TA Q500, TA Instruments) and the measurements were carried out from  $25^{\circ}\text{C}$  to  $600^{\circ}\text{C}$  at  $10^{\circ}\text{C}/\text{min}$  heating rate, and synthetic air (80%  $\text{N}_2$ / 20%  $\text{O}_2$ , flow rate 60 mL/min) was used as a purge gas.

### Alendronate Release from Scaffolds

Scaffolds of  $50 \pm 5\text{ mg}$  were incubated with 1 mL of distilled water. The full volume of water was replaced with fresh distilled water at specific time intervals. The collected supernatant was stored in a  $-20^{\circ}\text{C}$  freezer upon analysis. The stock solution of ALN was prepared by dissolving 20 mg of o-phthalaldehyde (OPA) in 19.9 mL of 0.05 M NaOH and 0.1 mL of 2-mercaptoethanol. The solution was used immediately. The samples containing 100  $\mu\text{L}$  of sample or blank ALN solution were combined with 150  $\mu\text{L}$  of OPA, and reacted for 2 hours. The release was calculated as a relative cumulative release. All samples were analyzed in 4 repetitions.

## Cell Isolation

### rOBs Isolation

Rat osteoblasts (rOBs) were isolated from either osteoporotic or control rats. For the exact procedure, animal treatment, and ethics see section Animal model and design of in vivo experiment. Femur bone fragments were enzymatically digested by  $5\times$  trypsin-EDTA solution (SAFC Biosciences, USA) for 10 min at  $37^{\circ}\text{C}$ , while shaking. The supernatant was discarded and bone fragments were rinsed with Dulbecco's modified Eagle's medium (DMEM; Merck, USA) with 1% Penicillin/Streptomycin (P/S). Secondly, bone fragments were digested in 300 U/mL of collagenase I (Gibco, USA) solution in DMEM for 30 min at  $37^{\circ}\text{C}$ , while shaking. The supernatant was discarded, the bone fragments were rinsed with DMEM with P/S, and then digested once more with collagenase I. The bone fragments were transferred to a culture flask coated with Collagen Coating Solution (Merck, USA), and cultured in DMEM supplemented with 10% fetal bovine serum (FBS) and 1% P/S.

### rPBMCs Isolation

Rat peripheral blood mononuclear cells (rPBMCs) were isolated from whole-blood aspirated from either the control or osteoporotic rats (for details see Animal model and design of in vivo experiment) by cardiac puncture under the inhalation of isoflurane. The peripheral blood with anticoagulants was diluted 1:1 in Hanks' balanced salt solution (HBSS), and layered over Ficoll-Paque and centrifuged for 30 min at  $360 \times g$  (NF800R centrifuge, Nüve, Ankara, Turkey) in a swing-out rotor. The mononuclear cell layer was aspirated, transferred into a conical tube, mixed with HBSS, and centrifuged for 10 min at  $407 \times g$  at  $16^{\circ}\text{C}$ . HBSS was added and repeated twice with the centrifugation steps: 10 min at  $282 \times g$  and 10 min at  $115 \times g$  at  $16^{\circ}\text{C}$ . Finally, the cells were mixed with DMEM (EuroClone, Italy), 2 mM L-glutamine (Gln), 10% FBS, and 1% P/S.

## Cell Seeding

The scaffolds 6 mm in diameter were sterilized using UV (for 20 min each side). The scaffolds were tested in terms of cytotoxicity, cell proliferation and osteogenic differentiation. Furthermore, we used co-cultures of rOBs (P1) and rPBMCs isolated from the control and osteoporotic rats. All cells were cultured in 5%  $\text{CO}_2$  at  $37^{\circ}\text{C}$ . Detailed culture conditions, scaffold type, and the source of cells used for in vitro experiments are listed in Table 1.

### Saos-2 Monoculture

The biocompatibility of scaffolds was tested on the culture of a Saos-2 osteosarcoma cell line (ATCC, LGC Standards). Scaffolds were seeded with  $2 \times 10^4$ /cells/scaffold in McCoy's medium supplemented with 15% FBS and 1% P/S.

**Table 1** Sample Naming List, Culture Conditions and the Source of Cells Used for in vitro Experiments

Group Name	Labeling for Release Study	HA	ALN	M-CSF and RANKL	Cell Source
PCL/ALN_C+MR	S1	-	+	+	Control rat
PCL/HA/ALN_C+MR	S2	+	+	+	Control rat
PCL/ALN_OP+MR	S1	-	+	+	Osteoporotic rat
PCL/HA/ALN_OP+MR	S2	+	+	+	Osteoporotic rat
PCL/ALN_C-MR	S1	-	+	-	Control rat
PCL/HA/ALN_C-MR	S2	+	+	-	Control rat
PCL/ALN_OP-MR	S1	-	+	-	Osteoporotic rat
PCL/HA/ALN_OP-MR	S2	+	+	-	Osteoporotic rat

**Abbreviations:** ALN, alendronate; C, control animal; HA, hydroxyapatite; M-CSF, macrophage colony-stimulating factor; OP, osteoporotic animal; PCL, polycaprolactone; RANKL, receptor activator of nuclear factor kappa B ligand.

### rOBs/rPBMCs Co-Culture

rOBs were seeded on scaffolds in 20  $\mu$ L of culture media in a density of  $3 \times 10^3$ /scaffold. The cells were then left to adhere for 2 hours, and the culture media (DMEM, 10% FBS, 1% P/S) was added. The following day, the medium was aspirated, and rPBMCs in 20  $\mu$ L of culture media were added on to the scaffolds with rOBs in a density of  $6 \times 10^4$ /scaffold. After 2 hours, the media was aspirated and a fresh culture media with 25 ng/mL of macrophage colony-stimulating factor (M-CSF) was added. The culture media for co-cultures consisted of 1:1 ratio of DMEM (EuroClone) with 2 mM Gln and DMEM (Merck), supplemented with 10% FBS and 1% P/S. The following day, marked as day 1, the media was aspirated and media with 25 ng/mL of M-CSF and 30 ng/mL of RANKL were added. Half of the volume of the culture media was changed every three days.

## In vitro Experiments

### Metabolic Activity and DNA Quantification

The metabolic activity of cells was measured using an MTS assay (CellTiter 96<sup>®</sup> Aqueous One Solution Cell Proliferation Assay; Promega, Madison, WI, USA), according to the manufacturer's manual. The absorbance at 490 nm and 690 nm was detected (Infinite M200 PRO; Tecan, Switzerland). Scaffolds were then transferred to the lysis buffer (0.2% v/v Triton X-100, 10 mM Tris (pH 7.0), and 1 mM EDTA), 200  $\mu$ L for monocultures, 100  $\mu$ L for co-cultures. After three freeze-thaw cycles, the amount of DNA was measured using the Quant-iT<sup>™</sup> dsDNA Assay Kit at ex./em. 485/523 nm (Life Technologies, Eugene, OR, USA) according to the manufacturer's manual.

### Confocal Microscopy

The samples were fixed with frozen methyl alcohol ( $-20^{\circ}\text{C}$ ) and incubated with 3,3'-diethyloxycarbocyanine iodide (DiOC6(3), Invitrogen, 20 mM diluted 1000x in PBS) for 45 min to visualize the internal membranes. Subsequently, the cell nuclei were stained using propidium iodide (PI; 5  $\mu$ g/mL in PBS, 10 min). The scaffolds were washed with PBS, and visualized using confocal microscopy (ZEISS LSM 5 DUO, PI:  $\lambda_{\text{ex}}=561$  nm,  $\lambda_{\text{em}}=630-700$  nm; DiOC6(3):  $\lambda_{\text{ex}}=488$  nm,  $\lambda_{\text{em}} = 505-550$  nm).

### Carbonic Anhydrase II Assay

The activity of carbonic anhydrase II (CA II) was evaluated from the cell lysate. Cells were lysed in 100  $\mu$ L of lysis buffer. The samples were frozen, thawed and vortexed. 50  $\mu$ L of cell lysate was mixed with 50  $\mu$ L of reaction buffer (12.5 mM TRIS, 75 mM NaCl, 2 mM 4-nitrophenyl acetate; pH = 7.5) and measured at 405 nm after one hour. The calibration curve was obtained from 4-nitrophenol, following the same protocol as with the samples.

### TRAP/ALP Assay

Tartrate-resistant acid phosphatase/alkaline phosphatase (TRAP/ALP) Assay kit (MK301, TaKaRa, Saint-Germain-en-Laye France) was used in accordance with the manufacturer's manual. The absorbance at 405 nm was detected using spectrophotometer (Infinite M200 PRO; Tecan, Switzerland).

## In vivo Testing

### Animal Model and Design of in vivo Experiment

All the experimental procedures were approved by the Animal Welfare Advisory Committee of the Ministry of Education, Youth and Sports of the Czech Republic (approval ID MSMT-10320/2019-3) and conducted under the supervision of the Animal Welfare Advisory Committee of the Charles University Faculty of Medicine in Pilsen following the technological, hygienic, welfare and ethical standards given by Directive 2010/63/EU and FELASA Guidelines and Recommendations (The workplace accreditation number 3456/2021-MZE-18134). In order to model a situation which is similar in humans, female Wistar rats aged 7–9 months that had undergone two or three births were used for the experiment. The animals received standard care according to EU directive 2010/63/EU, were fed ad libitum with complete granulated food (Sniff, Germany) and had free access to water. The light/dark cycle was 12h/12h. The rats were housed individually, in cages of type 3H (800 cm<sup>2</sup>; Bioscape, Germany).

The animals were divided into 12 experimental groups (n = 8; Table 2). A both side ovariectomy (OVX) was used to induce osteoporosis. Animals without OVX were used as a control. Two types of implants were used, PCL/HA and PCL/HA/ALN. An empty defect was used as a control. Systemic treatment with ALN was used for imitation of the human medicine approach in one part of the experimental groups.

### Induction of Osteoporosis

The OVX for the induction of osteoporosis was performed at the age 7–9 months. The animals were administered with isoflurane (3.0–3.5%) in oxygen using an anesthetic machine (Vetnar 1100, Grimed). Following the elevation of the abdominal wall of the restrained animal, the anesthetic mixture consisting of propofol (100 mg/kg; Propofol - Lipuro 2%, B. Braun), medetomidine (0.1 mg/kg; NarcoStart<sup>®</sup>, Produlab Pharma B.V.), and nalbuphine (0.1 mg/kg; Nalbuphin Orpha, Orpha-Devel Handels und Vertriebs GmbH) was administered peritoneally.

The bilateral ovariectomy was performed from lateral approaches. After removal of the ovary using absorbable surgical fiber for ligation, the surgical wound was sutured in two layers. The general anesthesia was then terminated by means of an i.m. injection of atipamezole (0.5 mg/kg; NarcoStop<sup>®</sup>, Produlab Pharma B.V., Raamsdomksveer, The Netherlands). Following surgery, the animals were provided with analgesia for 4 days using tramadol (12.5 mg/kg; Tramal<sup>®</sup>, STADA Arzneimittel AG, Bad Vilbel, Germany) and carprofen (5 mg/kg; Rimadyl<sup>®</sup>, Zoetis, Sao Paulo, Brazil).

### Scaffold Implantation and Further Treatment

After 5 months, the control and OVX animals were implanted with the scaffold into the bone. This surgical procedure was performed using the same anesthesia and analgesia scheme as described above. A standard hole (1.75 mm in

**Table 2** The List of Experimental Groups Used in the in vivo Study


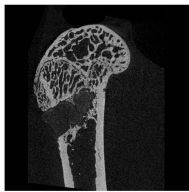
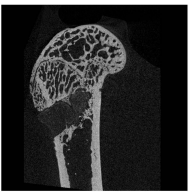
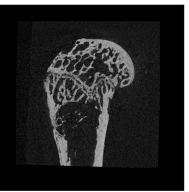



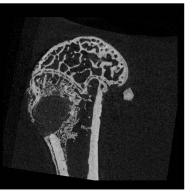

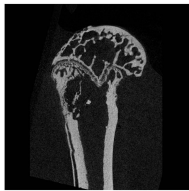
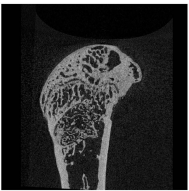
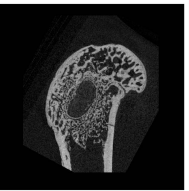


Group Name	Animals	Implanted Scaffold	Systemic Treatment with ALN
<b>PCL/HA_OP-ALN</b>	Osteoporotic	PCL/HA	-
<b>PCL/HA/ALN_OP-ALN</b>	Osteoporotic	PCL/HA/ALN	-
<b>Empty_OP-ALN</b>	Osteoporotic	Empty defect	-
<b>PCL/HA_C-ALN</b>	Control	PCL/HA	-
<b>PCL/HA/ALN_C-ALN</b>	Control	PCL/HA/ALN	-
<b>Empty_C-ALN</b>	Control	Empty defect	-
<b>PCL/HA_OP+ALN</b>	Osteoporotic	PCL/HA	+
<b>PCL/HA/ALN_OP+ALN</b>	Osteoporotic	PCL/HA/ALN	+
<b>Empty_OP+ALN</b>	Osteoporotic	Empty defect	+
<b>PCL/HA_C+ALN</b>	Control	PCL/HA	+
<b>PCL/HA/ALN_C+ALN</b>	Control	PCL/HA/ALN	+
<b>Empty_C+ALN</b>	Control	Empty defect	+

**Abbreviations:** ALN, alendronate; C, control animal; HA, hydroxyapatite; OP, osteoporotic animal; PCL, polycaprolactone.

diameter and depth 3.8 mm) was created in the lateral knee condyle of the left hind leg using a dental cutter and filled with the tested material. The rectangles of the tested nanofibrous layers with size 3.8×15 mm sterilized using ethylene oxide, were rolled up in the cylinders to fit in the prepared defect. The surgical wound was closed with an absorbable suture in anatomical layers. The rats from the experimental groups with systemic treatment with ALN were administered with 3.5 mg/kg of ALN per week (corresponding to dose 0.5 mg/kg/day) in drinking water calculated for the day consumption. The systemic treatment began with the implantation and continued during the whole 6 weeks.

### Micro-CT

Specimens (4 samples from each group) were scanned using desktop micro-CT SkyScan 1272 (Bruker micro-CT, Belgium). Specimens were immersed in 70% ethanol and scanned in plastic tubes with the following parameters: pixel size of 8  $\mu\text{m}$ , source voltage 80 kV, source current 125  $\mu\text{A}$ , 1 mm Al filter, frame averaging (2), rotation step 0.2°, rotation 180°. The flat-field correction was updated before each acquisition. Image data were reconstructed using NRecon. Cross-section images in selected orientation were achieved using DataViewer. Data were image-processed to reduce image noise. Data processing was optimized using TeIGen software.<sup>21</sup> D analysis of selected parameters (volume and surface) was performed via CTAn (Bruker). Semiquantitative evaluation of the healing of bone defects was assessed for: cortical bone healing, trabecular bone healing, bone surrounding former defect and overall evaluation. Healing was scored from 1 (poor) to 3 (excellent) except overall evaluation, which was scored from 1 (poor) to 4 (excellent). Illustration of semiquantitative evaluation is presented in Figure 1.

Rating		Cortical bone healing	Trabecular bone healing	Bone surrounding former defect	Overall evaluation
Low  ↑ ↓ Excellent	1				
	2				
	3				
	4				

**Figure 1** Semiquantitative evaluation of bone defect healing was assessed for: cortical bone healing, trabecular bone healing, bone surrounding former defect and overall evaluation. Healing was scored from 1 (poor) to 3 (excellent) except overall evaluation, which was scored from 1 (poor) to 4 (excellent).

## Histology

Harvested samples of distal femurs were fixed in 10% formol and after micro-CT scanning of selected representative samples, they were decalcified in Biodec-R (Bio-Optica). Decalcified samples were embedded in paraffin and 7  $\mu\text{m}$  sections were prepared using Leica RM2245 semi-automated rotary microtome (Leica). Sections were stained with Masson's green trichrome to visualize collagen in the tissue, dehydrated and covered using DPX mounting medium for histology (Sigma-Aldrich). The samples of a bone defect area were documented using Olympus BX61VS histology scanner and details were photographed using DMLB Leica microscope equipped with Leica MC170 HD camera.

## Statistical Analysis

Quantitative data from the in vitro analysis are presented as mean values  $\pm$  standard deviation (SD). The averaged values were determined from at least 4 independently prepared samples. The results were evaluated statistically using GraphPad Prism 9.1.1 (225). If the data passed the normality test, the statistical significance between a pair of groups was determined by ANOVA test and Tukey's comparative test for post-hoc analysis. If the data were without normal distribution, the statistical significance between a pair of groups was determined using Dunn's multiple comparison test for post-hoc analysis. For comparing two groups, unpaired *t*-test was used. All results were considered statistically significant if *p* was  $<0.05$ .

## Results

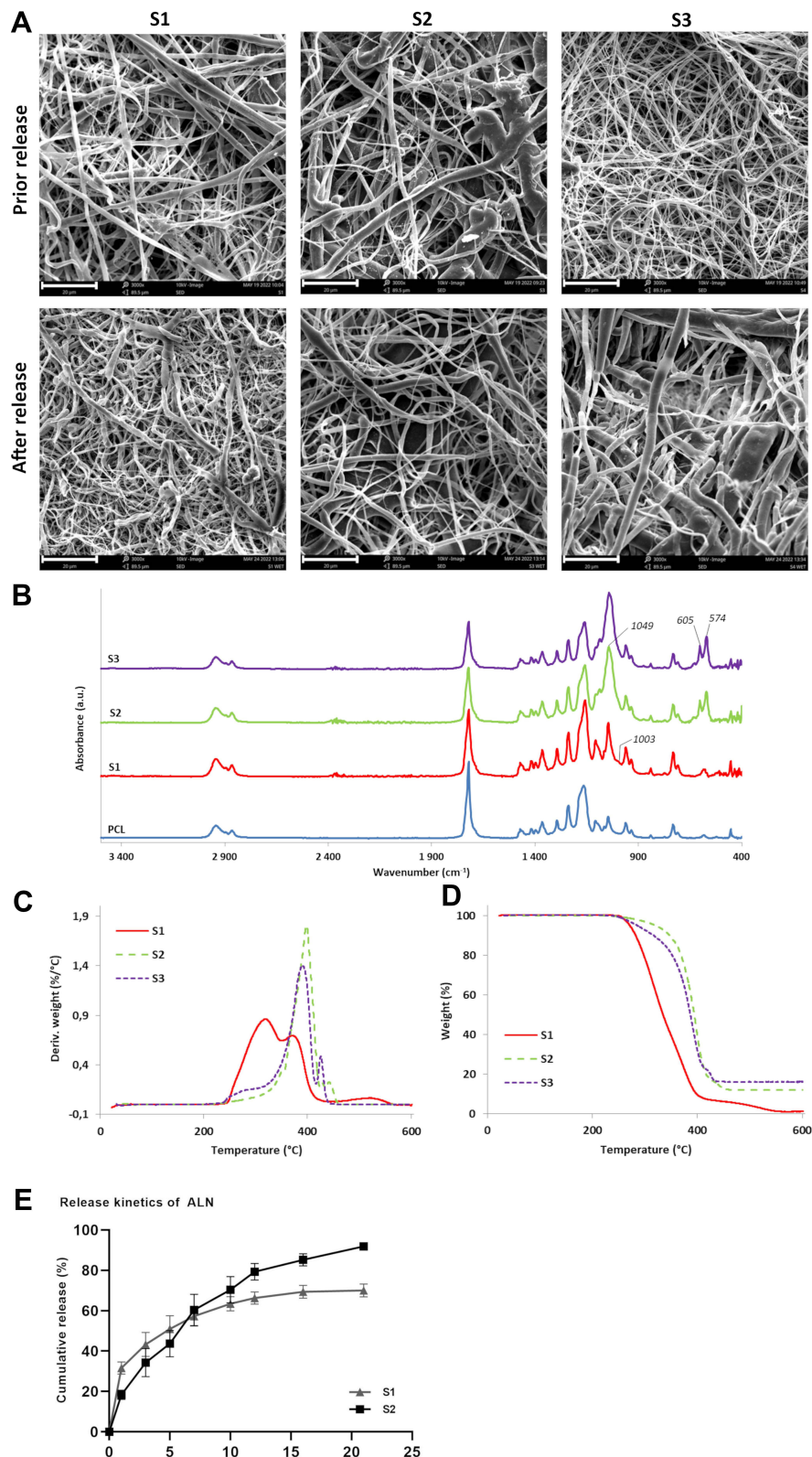
### Characterization of Scaffold, Release Study

In tissue engineering, the porous and fibrous scaffolds offer contact points suitable for cell adhesion and space for cell proliferation. The electrospun scaffolds showed nanofibrous morphology with the presence of microfibers (Figure 2A). The morphology among the samples did not deviate. The mean fiber diameter of the nanofibrous part was  $320 \pm 158$  nm and the microfibrillar part was  $3200 \pm 1850$  nm. The morphology prior and after 30 days incubation in distilled water did not result in a change of morphology or scaffold degradation.

Presence of HA on the scaffolds S2 and S3 was detected by ARS staining, FTIR and TGA analysis. The FTIR spectroscopy was used to observe the spectral changes and the representative bands of the spectra for the samples S1 – S3 with different composition. These were compared to FTIR spectra of pure PCL nanofibres and apatite library compounds. Obtained spectra are depicted in Figure 2B. All the FTIR spectra exhibit similarities related to the main component (PCL), which can be observed at  $3000\text{--}2800$   $\text{cm}^{-1}$  and around  $1720$   $\text{cm}^{-1}$  and are attributed to C-H vibrations and C=O stretching vibrations. All tested samples also contain peaks at  $1470\text{--}1360$   $\text{cm}^{-1}$  related to  $\text{CH}_2$  bending vibrations, C-O-C stretching vibrations peaks at  $1159$   $\text{cm}^{-1}$  and  $1236$   $\text{cm}^{-1}$  and C-O and C-C stretching vibrations related to a peak at  $1290$   $\text{cm}^{-1}$ . Differences in the compared spectra were observed mainly at  $1049$   $\text{cm}^{-1}$ ,  $605$   $\text{cm}^{-1}$  and  $574$   $\text{cm}^{-1}$ . These vibrations are attributed to apatite compounds – namely to the phosphate-related vibrations, and are present predominantly in samples S2 and S3. Minor changes in vibrations at  $1100\text{--}1000$   $\text{cm}^{-1}$  are also related to C-O-C and C-O vibrations and can be attributed to the presence of PF68 and other additives in samples S1 – S3.

TGA thermograms are shown in Figure 2C and D. Significant difference between sample S1 and samples S2, S3 was observed as confirmed by residual weight loss (%) and weight derivative ( $\%/^{\circ}\text{C}$ ) curves. The sample S1 underwent the most significant weight loss between  $250^{\circ}\text{C}$  and  $400^{\circ}\text{C}$  with weight derivative peaks maximum at  $318.66^{\circ}\text{C}$  and  $371.55^{\circ}\text{C}$ . In the case of samples S2 and S3, the most significant weight loss continued up to  $450^{\circ}\text{C}$  with peak maximums at  $398.21^{\circ}\text{C}$ ,  $427.93^{\circ}\text{C}$  and  $441.48^{\circ}\text{C}$  for sample S2 and  $391.21^{\circ}\text{C}$  and  $426.18^{\circ}\text{C}$  for sample S3. The overall weight residues after reaching  $600^{\circ}\text{C}$  were 1.258% for S1, 12.15% for S2 and 16.25% for S3. Increase of residual weight in case of samples S2 and S3 can be attributed to content of inorganic compounds (eg, HA) in their structure. Detailed TGA thermograms of each individual sample are listed in the [Supplementary Figure 1A-C](#). Moreover, ARS staining ([Supplementary Figure 1E-G](#)) showed that samples S2 and S3 were stained in red due to the presence of HA representing mineralization, while S1 scaffold remained unstained.

The ALN release from the fibrous scaffolds S1 and S2 lasted for 3 weeks. The release kinetics of ALN showed differences based on scaffold composition (Figure 2E). The samples with emulsion of PCL with ALN without both HA



**Figure 2** Scanning electron microscopy of prepared scaffolds prior and after performing ALN release study (A), scale bar 20 μm. FTIR spectra of S1 (ALN+, HA-, P3IRI-), S2 (ALN+, HA+, P3IRI+) and S3 (ALN-, HA+, P3IRI+) samples compared to PCL nanofibres without incorporated additives (B). TGA thermographs of samples S1, S2 and S3 expressed as residual weight (%) (C) and weight derivative (%/°C) (D) curves. Cumulative release of ALN from the scaffolds (E). Sample S3 did not contain ALN; therefore, the release study was not performed.

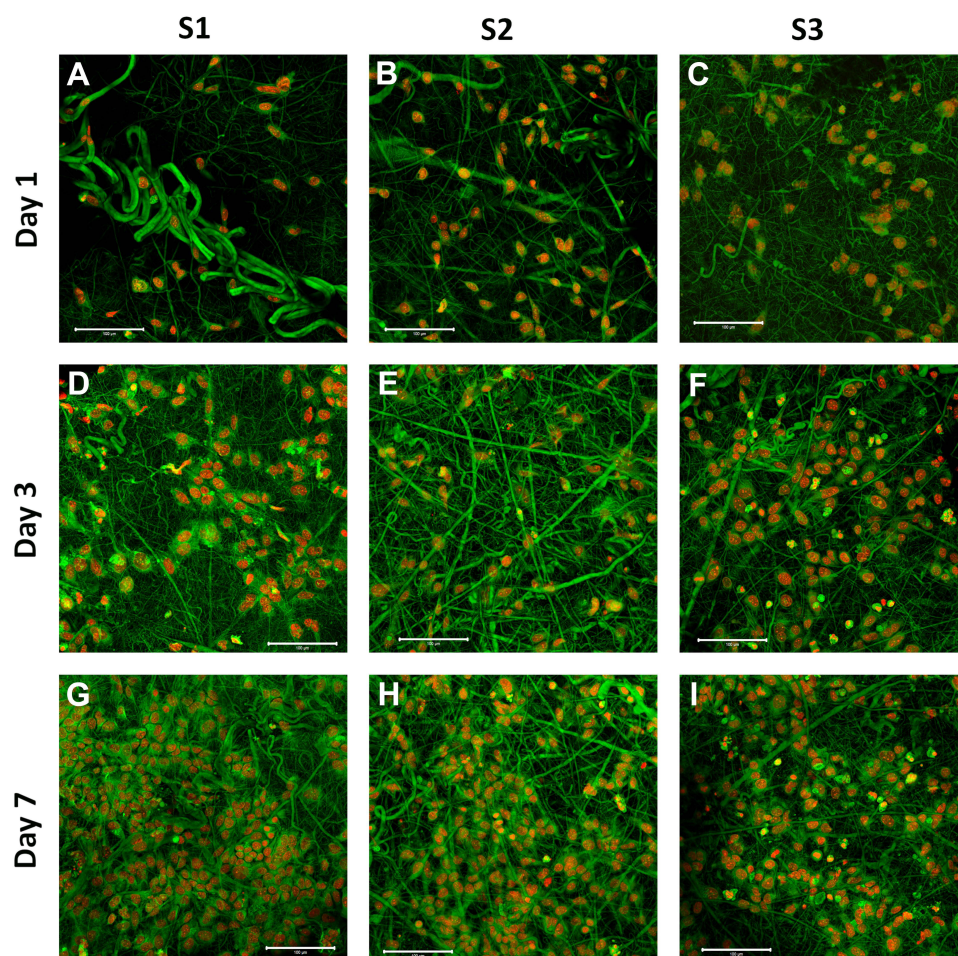


and pluronic P31R1 (S1) resulted in faster release, which was significantly higher compared to S2 ( $p = 0.0219$ ), followed by a stationary phase with statistically lower release compared to S2 since day 12. In the case of sample with ALN and both HA and P31R1 (S2), the release was accelerated and led to the complete elution of ALN in a 22-day period.

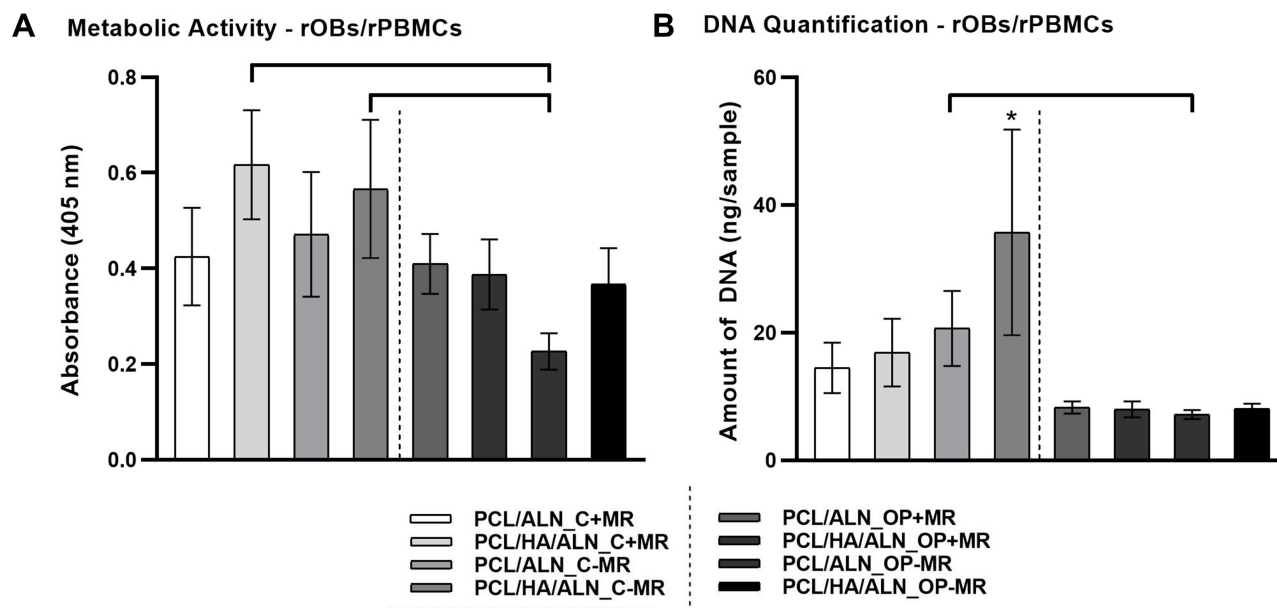
Based on the release study, scaffolds S1 and S2 represent different release kinetics during the 21-day release study. S1 was used for further in vitro study, named as PCL/ALN, as a model of burst release followed by a lower release rate compared to S2. S2 scaffold was used as a model of gradual long-time release and in further in vitro and in vivo studies was named as PCL/HA/ALN.

## In vitro Tests of Scaffold Biocompatibility, Osteogenic Potential and the Effect of Released ALN

The released ALN did not affect cell adhesion and proliferation. Biocompatibility of the scaffolds was proven using the culture of Saos-2 cells. The MTS test of Saos-2 cells showed no detrimental effect on either of the tested scaffolds, S1 (PCL/ALN) and S2 (PCL/HA/ALN) and S3 sample without ALN ([Supplementary Figure 2](#)). Furthermore, on day 1, well adhered and spread Saos-2 cells were detected by fluorescent microscopy staining ([Figure 3](#)). During the one-week culture period, the Saos-2 cells adopted typical spindle-like cell morphology, proving good biocompatibility of the scaffolds.



**Figure 3** Visualization of Saos-2 cells adhesion and distribution on scaffolds S1 (ALN+, HA-, P31R1-), S2 (ALN+, HA+, P31R1+) and S3 (ALN-, HA+, P31R1+) using confocal microscopy. Cell nuclei were stained by propidium iodide (red color) and cell internal membranes by DiOC6(3) (green color), scale bar 100  $\mu\text{m}$ . Sample S1, day 1 (**A**), S2, day 1 (**B**), S3, day 1 (**C**), S1, day 3 (**D**), S2, day 3 (**E**), S3, day 3 (**F**), S1, day 7 (**G**), S2, day 7 (**H**), S3, day 7 (**I**).



**Figure 4** Metabolic activity of rOBs/rPBMCs cells (A). DNA quantification of rOBs/rPBMCs cells (B). Statistical significance is denoted above the columns ( $p < 0.05$ ), \* means the statistically highest value.

To simulate the physiological interaction of bone cells on scaffolds, co-culture of cells isolated from the control and osteoporotic rats, rPBMCs and rOBs, was performed. rPBMCs were added in the culture of rOBs after 24 hours in the ratio rPBMCs:rOBs 20:1. Cells were co-cultured in the presence (+MR) or absence (-MR) of M-CSF and RANKL.

The fibrous scaffolds were not detrimental to the co-cultures of the cells, regardless of the different ALN release kinetics. The difference in metabolic activity and cell proliferation was related to the cell source. The metabolic activity was higher on PCL/HA/ALN\_C+MR and PCL/HA/ALN\_C-MR compared to PCL/ALN\_OP-MR (Figure 4A). The cell number was lower on the scaffolds seeded with cells isolated from osteoporotic animals, with no difference between these groups (Figure 4B). The highest cell number was detected on PCL/HA/ALN\_C+MR.

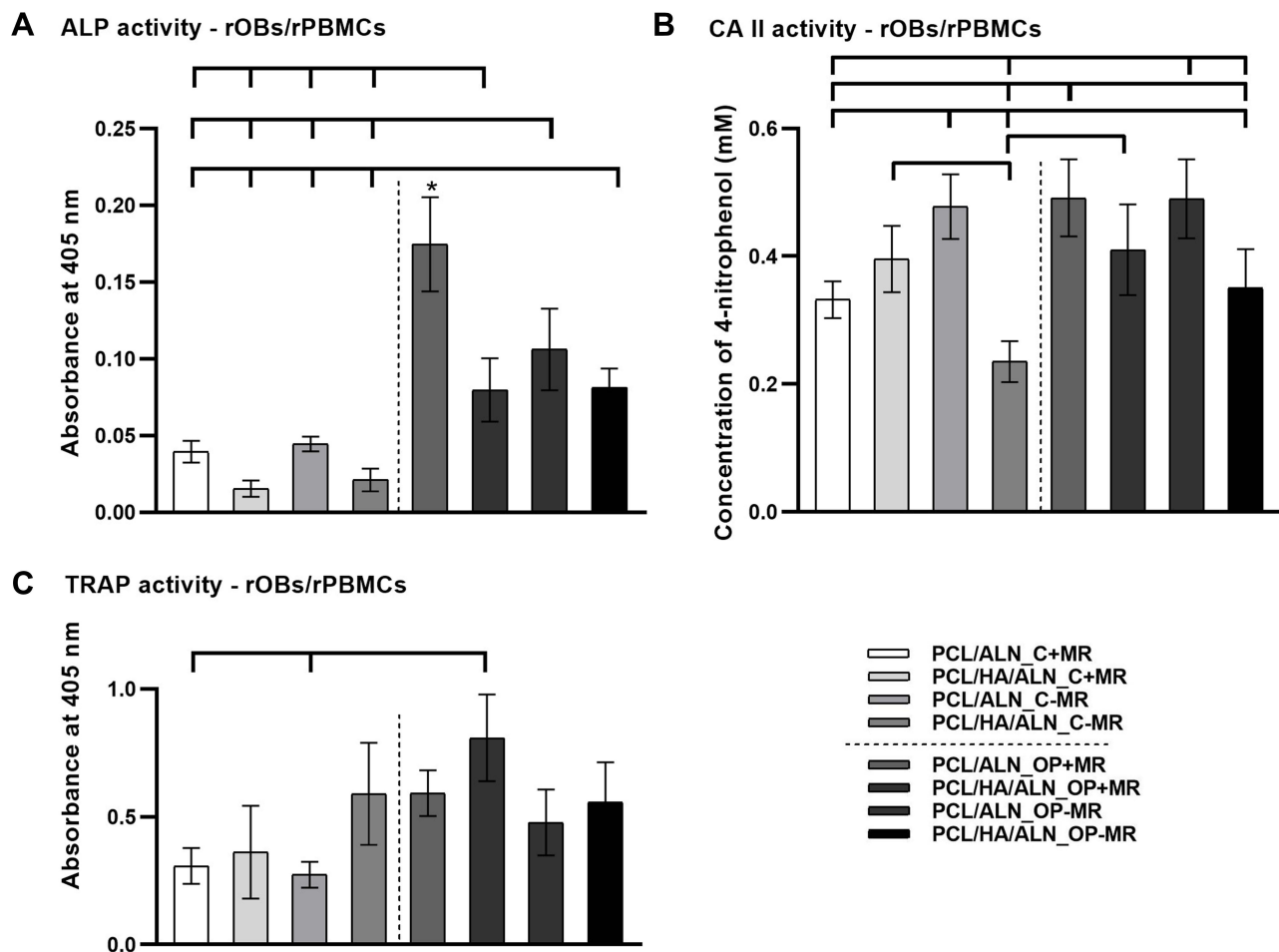
The ALP activity, an osteogenic marker, as well as CA II and TRAP activity, markers of osteoclastogenesis, were not affected by the different release kinetics of ALN. ALP was more active on the scaffolds seeded with cells isolated from osteoporotic rats, compared to control ones (Figure 5A). The highest ALP activity, compared to all groups, was detected on PCL/ALN\_OP+MR. The measurement of CA II activity did not show an unequivocal trend (Figure 5B). The highest CA II activity was measured on the samples without HA, PCL/ALN\_C-MR, PCL/ALN\_OP+MR and PCL/ALN\_OP-MR. The lowest value of CA II activity was detected on PCL/HA/ALN\_C-MR. TRAP activity was similar in all groups, except PCL/HA/ALN\_OP+MR, where the activity was higher compared to PCL/ALN\_C+MR and PCL/ALN\_C-MR (Figure 5C).

## In vivo Study

The animals were sacrificed 6 weeks after implantation of the scaffolds, and the bone samples were collected for further analysis. The defects were without any sign of inflammation. The defects were covered with connective tissue. In some defects of the groups with implanted scaffolds (PCL/HA and PCL/HA/ALN), the remnants of the scaffolds were still visible.

## Micro-CT Examination of Bone Defects

The micro-CT examination showed limited bone formation in the defects with the implanted non-degraded nanofibrous scaffolds, with higher dense trabeculae in the areas surrounding the scaffolds functionalized with ALN. The bone structure was clearly visible in micro-CT images (Figure 6). In most of the specimens the former bone defect is apparent and not completely healed. There are differences between the experimental groups, which can be seen in Figure 6. We



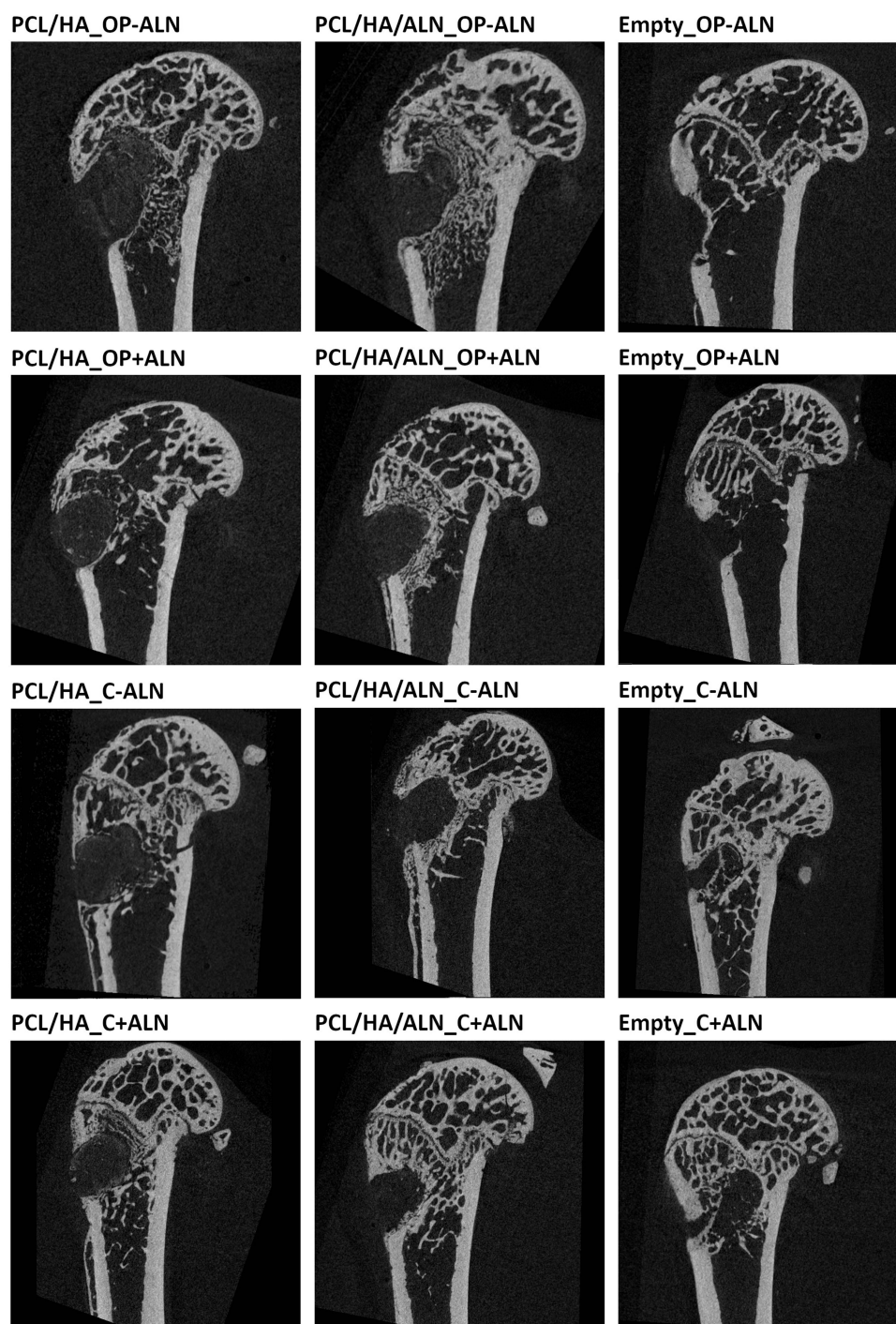
**Figure 5** ALP activity of rOBs/rPBMCs (A). CA II activity of rOBs/rPBMCs (B). TRAP activity of rOBs/rPBMCs (C) on day 10. Statistical significance is denoted above the columns ( $p < 0.05$ ), \*means the statistically highest value.

must consider that this figure presents only selected 2D sections, which we believe sufficiently represent the specimen structure. However, we evaluated specimens using 3D and 2D visualizations in many sections.

In some specimens, the residues of scaffold material may be seen. In certain images, mineralized tissue was observed inside the defect. Cortical bone healing is generally poor. Usually, there is healing from the borders of bone defects resulting in a variable reduction of the size of bone defect. Complete healing is observed only in the control specimens with no treatment at all (Figure 7A). However, even in these cases different cortical structure is evident (thinner or more porous). Even though there were visible differences between the experimental groups, the semiquantitative examination of the cortical bone did not prove any significant differences between the tested groups (Figure 7B).

The extent of trabecular bone healing is typically similar to cortical bone healing (Figure 7C). If there is a large cortical defect, trabecular healing is also poor. In some specimens, we may see partial trabecular healing even in the case of poor cortical healing. We assume that this could be explained by the variability of scaffold implantation in the defect, ie, the completeness of bone defect filling.

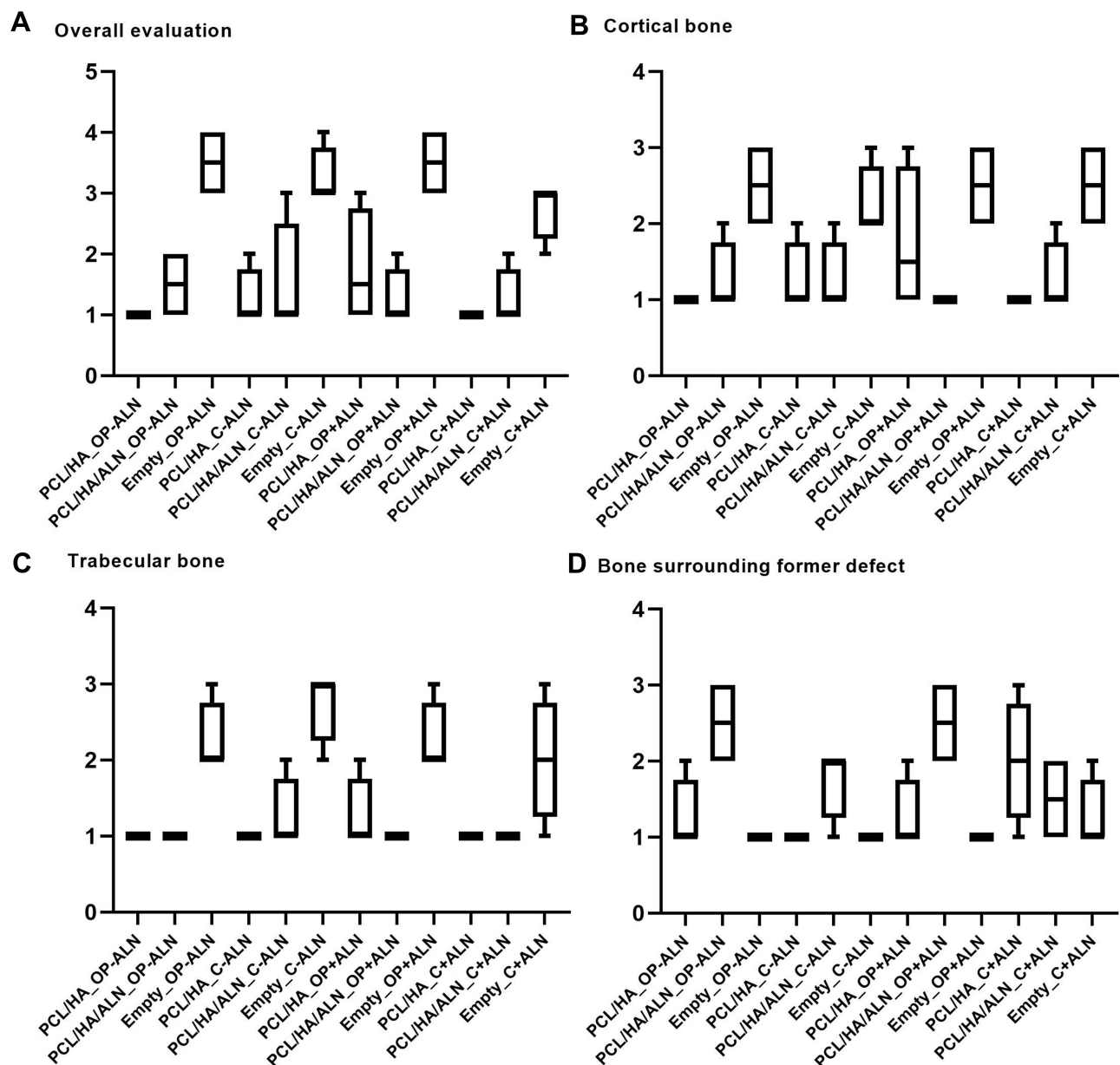
Large differences are observed in the bone structure which surrounds the former bone defect (Figure 7D). In many specimens, the surrounding bone consists of thin and dense bone trabeculae, which are highly interconnected. The thickness of this surrounding bone usually varies from 0.3 to 1.5 mm. The highest thickness presents specimens treated by PCL/HA/ALN, so we consider this to be the result of a local release of ALN from the implanted scaffolds. Systemic administration of ALN led to the formation of a similar bony structure, which was relatively thin.



**Figure 6** Micro-CT images of bone healing 6 weeks after implantation of the scaffolds.

### Histological Examination

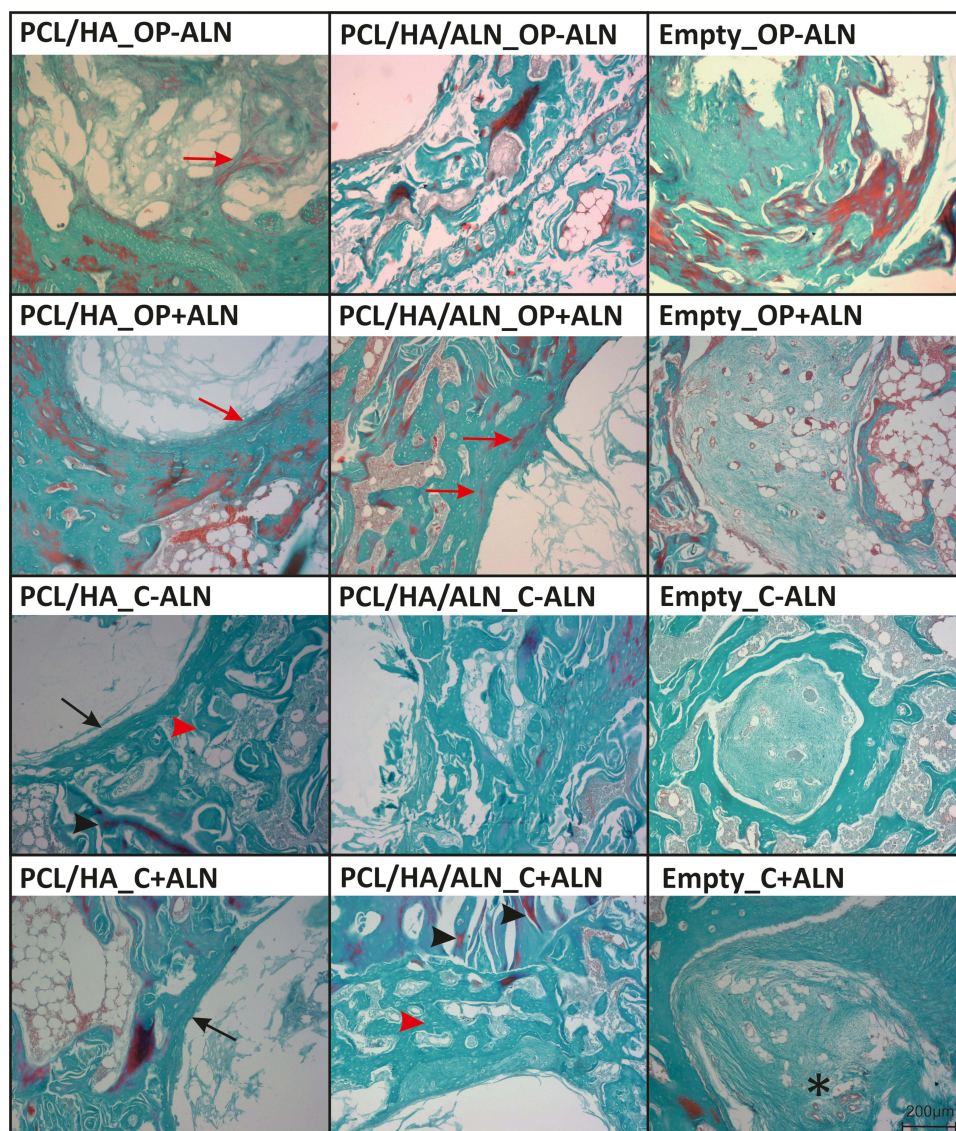
The histological examination showed similar results to the micro-CT analysis. The defect healing was evidently affected by the non-degraded scaffolds filling the defects; however, the new bone formation was more evident on the margins of the defects with the scaffolds releasing ALN. Masson's green trichrome was used to define new bone formation within a control or osteoporotic rat tibia critical size defect, containing a nanofibrous scaffold implanted for 6 weeks. All the experimental groups (Table 2) were generated (n = 8 per group).



**Figure 7** Semiquantitative evaluation of micro-CT images performed independently by 2 people. An evaluation of overall healing (A), cortical (B) and trabecular (C) bone as well as bone tissue surrounding the former bone defect (D) was performed.

By the sixth week post operation, all the groups showed marks of bone formation and calcification in the defect area (Figure 8). Observation of the Masson's green trichrome-stained sections showed areas of light green colored tissue of different thickness in the margins of the defects in all groups. New bone formation was apparent in the margins of the residual defects in different thickness from almost no healing signs (PCL/HA\_OP+ALN, PCL/HA\_C-ALN), to trabecular bone formation in the defect area extending from its margins to the center (PCL/HA/ALN\_C+ALN, empty defects). Interestingly, the presence of mineralized tissue directly inside the defect area was detected in the distinct groups (eg, PCL/HA\_OP-ALN).

In contrast to the groups with scaffolds, empty bone defects of the groups Empty\_C+ALN and Empty\_C-ALN were almost completely filled in. Mineralized osteoid was apparent in the major area and the residual central defects were filled with abundant connective tissue containing large numbers of blood vessels. In contrast to this, the empty defect of osteoporotic rats, Empty\_OP+ALN and Empty\_OP-ALN, were not completely closed even at 6 weeks after surgery, even



**Figure 8** Details of the partially healed defect area in different groups visualized in Masson's green trichrome-stained histological sections. The formation of new bone is apparent in the margins of the defects in all groups from woven bone of different thickness (black arrow) to the trabecular bone formation expanding from the margin of the defect to its center. The original matured bone (black arrowhead) is colored reddish in contrast to less mineralized new formed bone areas (red arrowhead). In the distinct groups, reddish areas of mineralized matrix (red arrow) were also apparent in the newly formed highly dense areas of woven bone in the margins of the bone defects or directly in the defect area. In the groups with empty defects without scaffold presence, the defect area was almost filled with new bone with remnants of the defect filled with connective tissue rich in blood vessels (asterisk).

if the new bone formation was more developed in comparison to the groups with scaffolds. Interestingly, the residual defect was broader in the osteoporotic group treated with ALN (Empty\_OP+ALN).

Newly formed woven bone or mineralized osteoid formation were observed in the margins of the defects. The woven bone area or calcified osteoid extended from the margins towards the center of the defect in a different brightness in different groups. In the bones of the control rats, the highest amount of new bone formation in the margins of the defect was observed in PCL/HA/ALN\_C+ALN, PCL/HA/ALN\_C-ALN groups. The lowest thickness of the new bone formation was apparent in the PCL/HA\_C-ALN group.

In the osteoporotic groups, the regeneration effect in the bone defects revealed a similar pattern. The areas of newly formed bone were thicker in PCL/HA/ALN\_OP+ALN, PCL/HA/ALN\_OP-ALN, than in the PCL/HA\_OP+ALN and PCL/HA\_OP-ALN. Surprisingly, PCL/HA\_OP-ALN evinced higher new bone formation than the PCL/HA\_OP+ALN. Almost no new woven bone at the margin of the PCL/HA\_OP+ALN group was apparent at 6 weeks post operation.

None of the groups except the control empty defect groups (Empty\_C+ALN, Empty\_C-ALN), demonstrated obvious new bone formation in the whole area of the bone defect at six weeks after surgery.

## Discussion

The treatment of bone fractures in osteoporotic patients could be prolonged due to the dysregulation of the interplay between OBs and osteoclasts. The aim of this study was to support the healing process by the drug delivery system, releasing ALN directly into the defect site.

The bone tissue has nano and micro structure morphology, which correlates with the structure of the electrospun fibrous and porous structure. Electrospinning is a versatile technique used to produce fibrous scaffolds.<sup>22</sup> Despite that nanofibrous scaffolds lack the mechanical properties of bone tissue, their fibrous nature mimics the natural cell environment. High surface to volume ration enables efficient protein adsorption<sup>23</sup> that precedes cell adhesion. At the same time, porosity of the scaffold with fibrous structure guarantee adopting the natural cell shape, and favors cell migration. Moreover, the versatility of the process enables incorporation of the drugs inside the nanofibers, and their subsequent sustained release.<sup>24,25</sup>

In this study, the electrospinning of PCL scaffolds resulted in the formation of nano/microfibrous scaffolds, which is typical for the PCL scaffolds processed from chloroform/ethanol solutions. The scaffolds showed similar morphology for all groups regardless of the chemical composition of fibers. Interestingly, the addition of HA does not result in any changes of fiber morphology indicating good dispersion. This finding is supported by the presence of HA particles on the surface of the scaffolds (Supplementary Figure 1D). Successful incorporation of HA within the scaffolds was proven by ARS staining which is used to detect the mineralization.<sup>26</sup> Moreover, chemical composition of electrospun nanofibres with ALN and HA was studied by FTIR and TGA analysis. Obtained results suggest successful incorporation and presence of HA in the samples S2 and S3, due to presence of  $\text{PO}_4^{3-}$  vibrations.<sup>27</sup> Content of ALN lies on detectable limit and therefore is not reliably provable by these methods. Under the FTIR examination, peaks typical for the PCL were observed in all samples at  $2949\text{ cm}^{-1}$  and  $2865\text{ cm}^{-1}$  due to  $\text{CH}_2$  stretching vibrations and in area  $1470\text{--}1360\text{ cm}^{-1}$  due to  $\text{CH}_2$  bending vibrations. The FTIR spectra also contained C-O-C stretching vibrations peaks at  $1159\text{ cm}^{-1}$  and  $1236\text{ cm}^{-1}$  and C-O and C-C stretching vibrations related peak at  $1290\text{ cm}^{-1}$ . These observations fully correspond with PCL nanofibres FTIR spectra provided by Canbolat et al.<sup>28</sup> FTIR spectra obtained for sample S1 (ALN+, HA-, P31R1-) does not show any significant deviations from pristine PCL nanofibres (without any additives). The only difference is at  $1003\text{ cm}^{-1}$ . This can be attributed to presence of additives, mainly pluronic, as observed in all samples S1, S2 and S3. In the case of S2 and S3 spectra, significant differences in FTIR spectra in comparison to S1 were observed at  $1049\text{ cm}^{-1}$ ,  $605\text{ cm}^{-1}$  a  $574\text{ cm}^{-1}$ , the peaks related to  $\text{PO}_4^{3-}$  vibrations, and can be attributed to HA incorporated into the nanofibres. ALN content, which should be also assigned to these vibrations, is below the detectable limit of the method.

These observations were supported by obtained TGA analysis results, where incorporation of HA led to increased residual weight at  $600^\circ\text{C}$  as significant thermal degradation of HA occurs above  $1000^\circ\text{C}$ .<sup>29</sup> The residues content was 12.15% in the case of S2 and 16.25% for S3 in contrast to the 1.258% in sample S1 without HA. The S1 thermogram exhibited curve typical for PCL nanofibers.<sup>28</sup> The 5% weight loss between  $450^\circ\text{C}$  and  $550^\circ\text{C}$  might be attributed to ALN content<sup>30</sup> in the sample S1 (ALN+, HA-, P31R1-). The 4.1% residual weight difference could be related to the same effect due to content of ALN in sample S2 (ALN+) and S3 (ALN-).

The electrospun nanofibers were prepared using emulsion needleless spinning. In order to increase the stability of water-in-oil emulsions, P31R1 was used. As reported by Novik et al, the addition of P31R1 helps to stabilize the liquid droplets on the interface with oil phase, and prolong the release times.<sup>31</sup> In this study, we prepared a combined nanoparticle dispersion and water-in-oil emulsion. During the scaffold fabrication, the P31R1 resulted in a worse spinning process and lower spinnability. The emulsion/dispersion stability was similar between the samples, and no phase separation issues were observed for the samples. The release studies showed faster release of ALN from the samples with P31R1. The differences were significant, resulting in a different total release rate.

In addition, the effect of HA nanoparticles on the release rate of ALN from emulsion-spun nanofibers was evaluated. The emulsion/dispersion type of nanofibers was formed. The release behavior of ALN from scaffolds indicated a burst release from the PCL scaffold without HA (S1) compared to sustained release from the sample S2 with HA, due to lower

diffusion spots in the emulsion-like structure of nanofibers without HA. The release in non-HA scaffold (S1) was governed by a diffusion mechanism/degradation mechanism. In the early phases, the release of ALN from the surface of the fibers was enabled by PF68/ALN water-leachable droplets connected to the surface, resulting in an immediate release. In later phases, the diffusion through these contact-spots was limited and the release was slower. Slow PCL degradation also caused the samples to show ~ 30% of non-released ALN content in the fibers after 22 days of incubation.

In the case of scaffolds with HA, the ALN release reached almost 90% after 22 days. The HA sequestered ALN and regulated the adsorption kinetics. Moreover, the anisotropic nature of the scaffold was further enhanced, creating diffusion routes for small molecular components. The behavior indicates an interaction between HA nanoparticles and ALN, diminishing and changing the behavior of emulsion compared to the samples without HA. Boanini et al showed interaction between HA and ALN.<sup>32</sup> In addition, thanks to the hydrophilic HA surface, the water phase upon interaction with its structure resulted in wetting of the surface and change to a non-emulsion form during the spinning process. Moreover, the SEM images demonstrate the surface localization of HA nanoparticles, creating a depot of ALN on their surface available for diffusion to the peri-implantation site. The release from HA containing scaffold was governed more by the absorption/desorption kinetics of ALN from HA, than by the diffusion/degradation mechanism observed in the scaffold without HA (S1). The presence of HA and P31R1 in S2 (ALN+, HA+, P31R1+) resulted in faster release compared to the scaffold without HA and P31R1 (S1), due to a further alternation of hydrophobic PCL surface by this O/W surfactant. The P31R1 wetted the hydrophobic PCL and HA surface and increased the ALN desorption rate from HA.

The effect of the different release kinetics of ALN was tested *in vitro* on co-cultures of osteoblasts and osteoclast-like cells, isolated from the osteoporotic and control rats. The *in vitro* testing of bone substitutes is commonly performed on monocultures of osteoblasts or differentiated MSCs. In this study, we used the co-cultures of primary osteoblasts and osteoclast-like cells to simulate the bone tissue complexity more accurately, as they are key players in bone formation and degradation. Only a limited number of studies used co-cultures to test bone substitutes.<sup>33–35</sup> The source of osteoblasts are primary cells isolated from bone tissue, osteosarcoma cell lines or differentiated MSCs. We isolated osteoblasts from adult rats with induced osteoporosis and control animals, using an explant isolation method with enzymatic pre-treatment.<sup>26</sup> Osteoclasts are mostly isolated as monocytes/macrophages and differentiated into osteoclasts during the culture.<sup>36</sup> Alternatively, cell lines, such as RAW or THP-1, can be used. Factors essential for osteoclastogenesis are M-CSF and RANKL.<sup>37</sup> In physiological conditions, osteoclastogenesis is regulated by osteoprotegerin (OPG), which competes for the binding of RANKL with RANK. If the balance between RANKL and OPG expression is impaired, diseases like osteoporosis evolve. Decreased estrogen production at menopause leads to an increased expression of RANKL and decreased expression of OPG.<sup>38</sup> In our study, we used primary PBMCs and induced osteoclast formation by the addition of M-CSF and RANKL to the culture medium.

The expected effect of the different ALN release kinetics, burst (S1) compared to gradual release (S2), on cell behavior was only partial. The measurement of metabolic activity and proliferation did not show any significant differences between either scaffold type. Difference was detected in CA II activity, but only when the co-cultures were cultured without RANKL and M-CSF. The cells cultured on scaffold S2, with sustained release of ALN, showed lower CA II activity. On the other hand, the measurement of TRAP activity did not confirm any differences between either group.

There are several studies concerning the effect of ALN on the inhibition of osteoclast activity. However, the effect varies based on the tested concentration of ALN. At low ALN concentrations, many of the published studies described that ALN supports proliferation, osteogenic marker expression and also increases the activity of osteoclast precursors, RAW cells or PBMCs. The effect of ALN concentration was tested on different cell types cultured on tissue culture plastic. The concentration of  $10^{-6}$  M was detected to be cytotoxic. The concentrations of  $10^{-7}$  M and  $10^{-10}$  M were described to have a positive effect on both osteoclastogenesis and osteogenic differentiation.<sup>16,39</sup>

Moreover, a similar effect of ALN on various cell types was observed, when gradually released from the scaffolds, indicating successful scaffold functionalization without the loss of the ALN therapeutic effect.<sup>16,20,40–42</sup>

Although the release study showed the different release kinetics of ALN, the effect did not manifest during the co-culture *in vitro* study. This could have been caused by the multiple exchange of the culture medium, which was necessary due to the needs of different media in different phases of the cell co-culture. It resulted in a partial wash out of the



released ALN. The release was faster in the scaffold S1, with a significant burst release. This means that the wash-out of the ALN was faster. Alternatively, the gradual release of S2 results in a higher concentration of ALN in the medium in later phases of the experiment, which was sufficient to decrease the CA II activity.

Interestingly, there was evident difference in the behavior of the co-cultured cells isolated from the osteoporotic and control animals. The co-culture of cells isolated from the osteoporotic animals showed a lower metabolic activity and proliferation, while the ALP activity was significantly higher in all the osteoporotic co-cultures compared to the control cells. The differences in cell behavior can be explained by the changes in osteoporotic bone metabolism. Ovariectomy causes decreased estrogen levels, leading to increased bone turnover.<sup>43–45</sup> Increased bone turnover leads to resorption of mature mineralized tissue and the formation of new tissue, which is not yet mineralized. Estrogen deficiency leads to bone resorption and the formation of imbalance, where resorption exceeds formation.<sup>46</sup> Increased bone turnover after ovariectomy in osteoporotic rats resulted in higher ALP activity of the isolated osteoblasts in comparison to control ones. Bone resorption and formation are coupled processes where signaling from osteoblasts to osteoclasts occurs and vice versa.<sup>47</sup> It means that when co-cultures were performed, osteoclast signaling to osteoblasts could have modulated their activity. Perinpanayagam et al observed poor initial adhesion of osteoporotic osteoblasts,<sup>48</sup> which most likely resulted in decreased proliferation. However, we did not observe poor cell adhesion of osteoporotic osteoblasts.

The PCL nanofibrous scaffold with gradual ALN release (S2, PCL/HA/ALN) was chosen for further in vivo testing. The scaffold without ALN was used as a control. Six weeks after implantation in the femur defects, the scaffolds were not completely degraded. The residual scaffolds filled the defects and limited new tissue formation. The areas of newly formed tissue were visible only in the margins of the defects treated with scaffolds and, in some samples of distinct groups, also small areas inside the defects. On the contrary, the empty defects of the control animals were filled completely.

The 6-week period was not sufficient for degradation of the PCL nanofibrous scaffold. The healing period was determined for 6 weeks to see the early effect of bone healing, which typically occurs in 6–8 weeks. The 6-week period is often chosen for these types of experiments.<sup>49,50</sup> Moreover, the release kinetics showed that most of the ALN is released in the first 22 days. The complete degradation of PCL typically occurs in a range of months or years.<sup>51,52</sup> On the other hand, the PCL degradation rate depends on the molecular weight and scaffold morphology, and could be accelerated for the finer scaffold structures.<sup>53,54</sup>

In this study, we expected a higher degradation rate, because the used polymer was of lower molecular weight (45 kDa). Moreover, the used electrospinning method enables the preparation of porous nanofibrous scaffolds with high surface to volume ratio and high porosity, enabling water uptake and subsequent ester bond hydrolysis. Enzymatic cleavage by lipases also occurs. The hydrolysis results in the loss of molecular weight; however, during this phase no weight loss of the polymer occurs. The weight loss occurs later when the fragments of polymers diffuse out.<sup>51</sup> In this study, the in vivo experiment lasted for 6 weeks. For the whole period, the PCL scaffolds retained their integrity; therefore, new bone formation was detected only in the margins of the defects.

The areas of woven bone or calcified osteoid extended towards the center differ through the groups with implanted scaffolds. The highest amount of new bone formation in the margins of the defect was observed in the groups with releasing ALN, regardless whether treated systematically with ALN. The concentration of ALN in the nanofibrous scaffold was 0.2 wt%. The total amount of ALN in the scaffold implanted in the defect was approximately 40 µg, with a gradual release for more than 22 days. In groups with implanted PCL/HA scaffolds without ALN, the new tissue formation in the margins was minimal. These results evidence the effect of released ALN on new bone tissue formation. This finding is in agreement with most of the published studies. The effect of ALN was tested on osteoporotic<sup>15–17,41</sup> and also control animals.<sup>18,19,55,56</sup>

In this study, we used the systematic administration of ALN to simulate the approach of human medicine to osteoporotic women. The rats were treated with 3.5 mg/kg of ALN once a week (which corresponds to the dose 0.5 mg/kg/day). Interestingly, the positive effect of ALN on bone tissue formation was described,<sup>19,57–59</sup> it was not confirmed in our study. The micro-CT and histological examination show similar results for the systematically treated and non-treated animals. Similarly, in line with our results, Weiss et al used ALN doses 1 mg/kg and 3 mg/kg three times a week and did not find any direct influence on the amount of bone neoformation. However, the administration of ALN

influenced the bone quality in a dose-dependent manner, ultimately affecting the distance and quantity of the trabeculae.<sup>60</sup>

The present study proves the effectiveness of the scaffold with incorporated ALN on the healing of the osteoporotic and healthy bone. Nevertheless, the degradation rate of the scaffold was not fast enough to enable new bone formation in the necessary time. The degradation rate could be adjusted by the combination of PCL with fast degraded polymer. We would consider these issues for future studies.

## Conclusion

We successfully prepared emulsion/dispersion scaffolds based on W/O emulsion of PCL and PF68 with ALN, containing HA nanoparticles as the dispersion phase. The HA and poloxamers enabled the control of ALN release kinetics without affecting the overall scaffold morphology. The ALN was gradually released from the scaffolds for more than 22 days. In the case of emulsion scaffolds without the dispersion phase, the release was slower with a sequestration of 40% of ALN in the fibers after 22 days. On the other hand, scaffolds with the emulsion/dispersion concept showed faster release and resulted in a 90% ALN release in 22 days. The scaffolds demonstrated the ALN effect on bone cells in vitro. Despite the slow degradation rate of the scaffold in vivo, the released ALN supported bone formation surrounding the implant residues and stimulated denser bone formation in the paracrine of the defect.

## Acknowledgments

This study was supported by the Czech Science Foundation (grant no. 18-09306S), Czech Health Research Council, grant no. NV18-05-00379, EU Horizon 2020 MSCA-RISE-2018 Research and Innovation Staff Exchange Program, project iP-OSTEO “Induced pluripotent stem cell for bone and cartilage defects” under the Marie Skłodowska-Curie grant agreement No 824007, by the project Cooperatio 207030 Dental Medicine/LF1, 207036-10 Morphological Disciplines of Medicine/LF1 and by the Ministry of Education, Youth and Sports of the Czech Republic and the European Union – European Structural and Investment Funds in the frames of Operational Programme Research, Development and Education – project Hybrid Materials for Hierarchical Structures (HyHi, Reg. No. CZ.02.1.01/0.0/0.0/16\_019/0000843). We would like to thank RESPILON Membranes s.r.o., Nove Sady 988/2, 602 00 Brno, Czech Republic for SEM analysis, Ing. Martin Stuchlík from Department of Nanochemistry, Institute for Nanomaterials, Advanced Technologies and Innovation, Technical University of Liberec for TGA and FTIR analysis, Assoc. prof. Tomáš Suchý for statistical consultation and Jakub Hedvičák for graphical editing.

## Disclosure

The authors report no conflicts of interest in this work.

## References

1. Kanis JA, Norton N, Harvey NC., et al. SCOPE 2021: a new scorecard for osteoporosis in Europe. *Arch Osteoporos*. 2021;16:82. doi:10.1007/s11657-020-00871-9
2. Torstrick FB, Guldberg RE. Local strategies to prevent and treat osteoporosis. *Curr Osteoporos Rep*. 2014;12:33–40. doi:10.1007/s11914-014-0191-6
3. Lufkin EG, Wahner HW, O’Fallon WM, et al. Treatment of postmenopausal osteoporosis with transdermal estrogen. *Ann Intern Med*. 1992;117:1–9. doi:10.7326/0003-4819-117-1-1
4. Ellerington MC, Hillard TC, Whitcroft SI, et al. Intranasal salmon calcitonin for the prevention and treatment of postmenopausal osteoporosis. *Calcif Tissue Int*. 1996;59:6–11. doi:10.1007/s002239900076
5. Henriksen K, Byrjalsen I, Andersen JR, et al. A randomized, double-blind, multicenter, placebo-controlled study to evaluate the efficacy and safety of oral salmon calcitonin in the treatment of osteoporosis in postmenopausal women taking calcium and vitamin D. *Bone*. 2016;91:122–129. doi:10.1016/j.bone.2016.07.019
6. Bone HG, Bolognese MA, Yuen CK, et al. Effects of denosumab on bone mineral density and bone turnover in postmenopausal women. *J Clin Endocrinol Metab*. 2008;93:2149–2157. doi:10.1210/jc.2007-2814
7. Langdahl BL, Libanati C, Crittenden DB, et al. Romosozumab (sclerostin monoclonal antibody) versus teriparatide in postmenopausal women with osteoporosis transitioning from oral bisphosphonate therapy: a randomised, open-label, Phase 3 trial. *Lancet*. 2017;390:1585–1594.
8. Glover SJ, Eastell R, McCloskey EV, et al. Rapid and robust response of biochemical markers of bone formation to teriparatide therapy. *Bone*. 2009;45:1053–1058. doi:10.1016/j.bone.2009.07.091

9. Turbí C, Herrero-Beaumont G, Acebes JC, et al. Compliance and satisfaction with raloxifene versus alendronate for the treatment of postmenopausal osteoporosis in clinical practice: an open-label, prospective, nonrandomized, observational study. *Clin Ther.* 2004;26:245–256. doi:10.1016/S0149-2918(04)90023-9
10. Wysowski DK, Greene P. Trends in osteoporosis treatment with oral and intravenous bisphosphonates in the United States, 2002–2012. *Bone.* 2013;57:423–428. doi:10.1016/j.bone.2013.09.008
11. Roelofs AJ, Thompson K, Gordon S, et al. Molecular mechanisms of action of bisphosphonates: current status. *Clin Cancer Res.* 2006;12(20):6222s–30s. doi:10.1158/1078-0432.CCR-06-0843
12. Ruggiero SL, Dodson TB, Assael LA, et al. American Association of Oral and Maxillofacial Surgeons position paper on bisphosphonate-related osteonecrosis of the jaws—2009 update. *J Oral Maxillofac Surg.* 2009;67:2–12. doi:10.1016/j.joms.2009.01.009
13. Lui PP, Lee YW, Mok TY, et al. Local administration of alendronate reduced peri-tunnel bone loss and promoted graft-bone tunnel healing with minimal systemic effect on bone in contralateral knee. *J Orthop Res.* 2013;31:1897–1906. doi:10.1002/jor.22442
14. Özer T, Aktas A, Baris E, et al. Effects of local alendronate administration on bone defect healing. Histomorphometric and radiological evaluation in a rabbit model. *Acta Cir Bras.* 2017;32:781–795. doi:10.1590/s0102-865020170090000010
15. van Houdt CIA, Gabbai-Armelin PR, Lopez-Perez PM, et al. Alendronate release from calcium phosphate cement for bone regeneration in osteoporotic conditions. *Sci Rep.* 2018;8:15398. doi:10.1038/s41598-018-33692-5
16. Wang X, Zeng D, Weng W, et al. Alendronate delivery on amino modified mesoporous bioactive glass scaffolds to enhance bone regeneration in osteoporosis rats. *Artif Cells Nanomed Biotechnol.* 2018;46:171–181. doi:10.1080/21691401.2018.1453825
17. Zeng Y, Zhou M, Chen L, et al. Alendronate loaded graphene oxide functionalized collagen sponge for the dual effects of osteogenesis and anti-osteoclastogenesis in osteoporotic rats. *Bioactive Mater.* 2020;5:859–870. doi:10.1016/j.bioactmat.2020.06.010
18. Bobyn JD, Thompson R, Lim L, et al. Local alendronate acid elution increases net periimplant bone formation: a micro-CT analysis. *Clin Orthop Relat Res.* 2014;472(2):687–694. doi:10.1007/s11999-013-3120-6
19. Tokar H, Ozdemir H, Ozer H, et al. Alendronate enhances osseous healing in a rat calvarial defect model. *Arch Oral Biol.* 2012;57(11):1545–1550. doi:10.1016/j.archoralbio.2012.06.013
20. Yun YP, Kim SJ, Lim YM, et al. The effect of alendronate-loaded polycaprolactone nanofibrous scaffolds on osteogenic differentiation of adipose-derived stem cells in bone tissue regeneration. *J Biomed Nanotechnol.* 2014;10:1080–1090. doi:10.1166/jbn.2014.1819
21. Jiřík M, Bartoš M, Tomášek P, et al. Generating standardized image data for testing and calibrating quantification of volumes, surfaces, lengths, and object counts in fibrous and porous materials using X-ray microtomography. *Microsc Res Tech.* 2018;81:551–568. doi:10.1002/jemt.23011
22. Yoshimoto H, Shin YM, Terai H, et al. A biodegradable nanofiber scaffold by electrospinning and its potential for bone tissue engineering. *Biomaterials.* 2003;24:2077–2082. doi:10.1016/S0142-9612(02)00635-X
23. Regis S, Youssefian S, Jassal M, et al. Fibronectin adsorption on functionalized electrospun polycaprolactone scaffolds: experimental and molecular dynamics studies. *J Biomed Mater Res A.* 2014;102(6):1697–1706. doi:10.1002/jbm.a.34843
24. Lukasova V, Buzgo M, Vocetkova K, et al. Osteoinductive 3D scaffolds prepared by blend centrifugal spinning for long-term delivery of osteogenic supplements. *RSC Adv.* 2018;8:21889–21904. doi:10.1039/C8RA02735H
25. Radisavljevic A, Stojanovic DB, Perisic S, et al. Cefazolin-loaded polycaprolactone fibers produced via different electrospinning methods: characterization, drug release and antibacterial effect. *Eur J Pharmaceutical Sci.* 2018;124:26–36. doi:10.1016/j.ejps.2018.08.023
26. Žižková R, Hedvičáková V, Blahnová VH, et al. The Effect of Osteoblast Isolation Methods from Adult Rats on Osteoclastogenesis in Co-Cultures. *Int J Mol Sci.* 2022;23(14):7875. doi:10.3390/ijms23147875
27. Mir M, Leite FL, Herrmann Junior PSDP. XRD, AFM, IR and TGA study of nanostructured hydroxyapatite. *Materials Res.* 2012;15(4):6. doi:10.1590/S1516-14392012005000069
28. Canbolat MF, Celebioglu A, Uyar T. Drug delivery system based on cyclodextrin-naproxen inclusion complex incorporated in electrospun polycaprolactone nanofibers. *Colloids Surf B Biointerfaces.* 2014;115:15–21. doi:10.1016/j.colsurfb.2013.11.021
29. Senra MR, Lima R, Souza J, et al. Thermal characterization of hydroxyapatite or carbonated hydroxyapatite hybrid composites with distinguished collagens for bone graft. *J Mater Res Technol.* 2020;9(4):7190–7200. doi:10.1016/j.jmrt.2020.04.089
30. Cicco SR, Vona D, Leone G, et al. In vivo functionalization of diatom biosilica with sodium alendronate as osteoactive material. *Mater Sci Eng.* 2019;104:109897. doi:10.1016/j.msec.2019.109897
31. Novik H, Clerici M, Fahmi A, et al. High-Throughput Electrospinning of Bioactive Scaffolds for Bone Regeneration. *Proceedings.* 2021;78:24.
32. Boanini E, Torricelli P, Gazzano M, et al. Alendronate-hydroxyapatite nanocomposites and their interaction with osteoclasts and osteoblast-like cells. *Biomaterials.* 2008;29(7):790–796. doi:10.1016/j.biomaterials.2007.10.040
33. Heinemann C, Heinemann S, Worch H, et al. Development of an osteoblast/osteoclast co-culture derived by human bone marrow stromal cells and human monocytes for biomaterials testing. *Eur Cell Mater.* 2011;21:80–93. doi:10.22203/eCM.v021a07
34. Dolci LS, Panzavolta S, Torricelli P, et al. Modulation of Alendronate release from a calcium phosphate bone cement: an in vitro osteoblast-osteoclast co-culture study. *Int J Pharm.* 2019;554:245–255. doi:10.1016/j.ijpharm.2018.11.023
35. Meng G, Wu X, Yao R, et al. Effect of zinc substitution in hydroxyapatite coating on osteoblast and osteoclast differentiation under osteoblast/osteoclast co-culture. *Regen Biomater.* 2019;6:349–359. doi:10.1093/rb/rbz001
36. Borciani G, Montalbano G, Baldini N, et al. Co-culture systems of osteoblasts and osteoclasts: simulating in vitro bone remodeling in regenerative approaches. *Acta Biomaterialia.* 2020;108:22–45. doi:10.1016/j.actbio.2020.03.043
37. Asagiri M, Takayanagi H. The molecular understanding of osteoclast differentiation. *Bone.* 2007;40:251–264. doi:10.1016/j.bone.2006.09.023
38. Owen R, Reilly GC. In vitro models of bone remodelling and associated disorders. *Front Bioeng Biotechnol.* 2018;6:134. doi:10.3389/fbioe.2018.00134
39. Hedvičáková V, Žižková R, Buzgo M, et al. The effect of alendronate on osteoclastogenesis in different combinations of M-CSF and RANKL growth factors. *Biomolecules.* 2021;12(1):11. doi:10.3390/biom12010011
40. Park KW, Yun YP, Kim SE, et al. The effect of alendronate loaded biphasic calcium phosphate scaffolds on bone regeneration in a rat tibial defect model. *Int J Mol Sci.* 2015;16:26738–26753. doi:10.3390/ijms161125982
41. Zeng Y, Zhou M, Mou S, et al. Sustained delivery of alendronate by engineered collagen scaffold for the repair of osteoporotic bone defects and resistance to bone loss. *J Biomed Mater Res A.* 2020;108:2460–2472. doi:10.1002/jbm.a.36997

42. Shen X, Ma P, Hu Y, et al. Alendronate-loaded hydroxyapatite-TiO<sub>2</sub> nanotubes for improved bone formation in osteoporotic rabbits. *J Mater Chem B*. 2016;4:1423–1436. doi:10.1039/C5TB01956G
43. Iwamoto J, Seki A, Matsuura M, et al. Influence of ovariectomy on bone turnover and trabecular bone mass in mature cynomolgus monkeys. *Yonsei Med J*. 2009;50:358–367. doi:10.3349/ymj.2009.50.3.358
44. Kennedy OD, Brennan O, Rackard SM, et al. Effects of ovariectomy on bone turnover, porosity, and biomechanical properties in ovine compact bone 12 months postsurgery. *J Orthop Res*. 2009;27:303–309. doi:10.1002/jor.20750
45. Zhang Y, Lai WP, Leung PC, et al. Short- to mid-term effects of ovariectomy on bone turnover, bone mass and bone strength in rats. *Biol Pharm Bull*. 2007;30:898–903. doi:10.1248/bpb.30.898
46. Väänänen HK, Härkönen PL. Estrogen and bone metabolism. *Maturitas*. 1996;23(Suppl):S65–9. doi:10.1016/0378-5122(96)01015-8
47. Khosla S, Oursler MJ, Monroe DG. Estrogen and the skeleton. *Trends Endocrinol Metab*. 2012;23:576–581. doi:10.1016/j.tem.2012.03.008
48. Perinpanayagam H, Zaharias R, Stanford C, et al. Early cell adhesion events differ between osteoporotic and non-osteoporotic osteoblasts. *J Orthop Res*. 2001;19(6):993–1000. doi:10.1016/S0736-0266(01)00045-6
49. Cheung WH, Miclaui T, Chow SK-H, et al. Fracture healing in osteoporotic bone. *Injury*. 2016;47(Suppl 2):S21–6. doi:10.1016/S0020-1383(16)47004-X
50. Thormann U, El Khawassna T, Ray S, et al. Differences of bone healing in metaphyseal defect fractures between osteoporotic and physiological bone in rats. *Injury*. 2014;45:487–493. doi:10.1016/j.injury.2013.10.033
51. Sajkiewicz P, Heljak MK, Gradys A, et al. Degradation and related changes in supermolecular structure of poly(caprolactone) in vivo conditions. *Polym Degrad Stab*. 2018;157:70–79. doi:10.1016/j.polymdegradstab.2018.09.023
52. Seyednejad H, Gawlitta D, Kuiper RV, et al. In vivo biocompatibility and biodegradation of 3D-printed porous scaffolds based on a hydroxyl-functionalized poly( $\epsilon$ -caprolactone). *Biomaterials*. 2012;33:4309–4318. doi:10.1016/j.biomaterials.2012.03.002
53. Bölgen N, Menceloğlu YZ, Acatay K, et al. In vitro and in vivo degradation of non-woven materials made of poly( $\epsilon$ -caprolactone) nanofibers prepared by electrospinning under different conditions. *J Biomater Sci Polym Ed*. 2005;16:1537–1555. doi:10.1163/156856205774576655
54. Sung HJ, Meredith C, Johnson C, et al. The effect of scaffold degradation rate on three-dimensional cell growth and angiogenesis. *Biomaterials*. 2004;25:5735–5742. doi:10.1016/j.biomaterials.2004.01.066
55. Garbuz DS, Hu Y, Kim WY, et al. Enhanced gap filling and osteoconduction associated with alendronate-calcium phosphate-coated porous tantalum. *J Bone Joint Surg Am*. 2008;90:1090–1100. doi:10.2106/JBJS.G.00415
56. Niu S, Cao X, Zhang Y, et al. Peri-implant and systemic effects of high-/low-affinity bisphosphonate-hydroxyapatite composite coatings in a rabbit model with peri-implant high bone turnover. *BMC Musculoskelet Disord*. 2012;13(1):97. doi:10.1186/1471-2474-13-97
57. Nakao S, Minamide A, Kawakami M, et al. The influence of alendronate on spine fusion in an osteoporotic animal model. *Spine*. 2011;36(18):1446–1452. doi:10.1097/BRS.0b013e3181f49c47
58. Oliveira D, Hassumi JS, Gomes-Ferreira PH, et al. Short term sodium alendronate administration improves the peri-implant bone quality in osteoporotic animals. *J Appl Oral Sci*. 2017;25:42–52. doi:10.1590/1678-77572016-0165
59. Im S, Lim SH, Lee JI, et al. Effective dosage and administration schedule of oral alendronate for non-nociceptive symptoms in rats with chronic constriction injury. *J Korean Med Sci*. 2010;25:938–944. doi:10.3346/jkms.2010.25.6.938
60. Weiss SG, Kuchar GO, Gerber JT, et al. Dose of alendronate directly increases trabeculae expansivity without altering bone volume in rat femurs. *World J Orthop*. 2018;9:190–197. doi:10.5312/wjo.v9.i10.190